NMNAT1 Is Essential for Human iPS Cell Differentiation to the Retinal Lineage

Hiroshi Kuribayashi,[1] Toshiro Iwagawa,[1] Akira Murakami,[2] Takeshi Kawamura,[3] Yutaka Suzuki,[4] and Sumiko Watanabe[1]

[1]Department of Retinal Development and Pathology, Graduate School of Medicine, The University of Tokyo, Bunkyo-ku, Tokyo, Japan
[2]Department of Ophthalmology, Graduate School of Medicine, Juntendo University, Tokyo, Japan
[3]Isotope Science Center, The University of Tokyo, Bunkyo-ku, Tokyo, Japan
[4]Department of Medical Genome Sciences, Graduate School of Frontier Science, The University of Tokyo, Bunkyo-ku, Chiba, Japan

Correspondence: Sumiko Watanabe, Department of Retinal Biology and Pathology, Graduate School of Medicine, The University of Tokyo, 7-3-1 Hongo, Bunkyo-ku, Tokyo 113-8655, Japan; sumiko@g.ecc.u-tokyo.ac.jp.

HK and TI equally contributed to this study.

Received: December 20, 2023
Accepted: September 27, 2024
Published: October 24, 2024

Citation: Kuribayashi H, Iwagawa T, Murakami A, Kawamura T, Suzuki Y, Watanabe S. NMNAT1 is essential for human iPS cell differentiation to the retinal lineage. *Invest Ophthalmol Vis Sci.* 2024;65(12):37. https://doi.org/10.1167/iovs.65.12.37

Purpose. The gene encoding nicotinamide mononucleotide adenylyltransferase 1 (NMNAT1), a nicotinamide adenine dinucleotide synthetase localized in the cell nucleus, is a causative factor in Leber's congenital amaurosis, which is the earliest onset type of inherited retinal degeneration. We sought to investigate the roles of NMNAT1 in early retinal development.

Methods. We used human induced pluripotent stem cells (hiPSCs) and established NMNAT1-knockout (KO) hiPSCs using CRISPR/cas9 technology to reveal the roles of NMNAT1 in human retinal development.

Results. NMNAT1 was not essential for the survival and proliferation of immature hiPSCs; therefore, we subjected NMNAT1-KO hiPSCs to retinal organoid (RO) differentiation culture. The expression levels of immature hiPSC-specific genes decreased in a similar manner after organoid culture initiation up to 2 weeks in the control and NMNAT1-KO. Neuroectoderm-specific genes were induced in the control and NMNAT1-KO organoids within a few days after starting the organoid culture; *PAX6* and *TUBB3* were higher in NMNAT1-KO organoids up to 7 days than in the control organoids. However, the induction of genes involving retinal early development, such as *RAX*, which was induced at around day 10 in this culture, was considerably reduced in NMNAT1-KO organoids. Morphological examination also showed failure of retinal primordial structure formation, which became visible at around 2 weeks of the control culture, in the NMNAT1-KO organoids. Decreased intracellular NAD levels and poly(ADP-ribosyl)ation were observed in NMNAT1-KO organoids at 7 to 10 days of the culture. Mass spectrometry analysis of inhibited proteins in the poly(ADP-ribosyl)ation pathway identified poly(ADP-ribosyl)ation of poly(ADP-ribose) polymerase 1 (PARP1) as a major protein.

Conclusions. These results indicate that NMNAT1 was dispensable for neural lineage differentiation but essential for the commitment of retinal fate differentiation in hiPSCs. The NMNAT1-NAD-PARP1 axis may play a critical role in the appropriate development of human retinal lineage differentiation.

Keywords: nicotinamide adenine dinucleotide (NAD), retina, retinal differentiation, human induced pluripotent stem cells (hiPSCs)

Nicotinamide mononucleotide adenylyltransferase (NMNAT) is one of multiple genes encoding nicotinamide adenine dinucleotide (NAD) synthetase. NMNATs are essential enzymes in NAD synthesis pathways, which catalyze the conversion of nicotinamide mononucleotide (NMN) to NAD or nicotinic acid mononucleotide (NaMN) to nicotinic acid adenine dinucleotide (NaAD). NAD is a critical co-substrate for NAD-dependent enzymes, such as sirtuins (SIRTs) and poly(ADP-ribose) polymerases (PARPs); it plays roles in multiple cell signaling pathways that contribute to development, homeostasis, and aging.[1,2]

The NMNAT family of genes comprises three isoforms: NMNAT1, NMNAT2, and NMNAT3. These isoform proteins exhibit different subcellular localization patterns in the nucleus, cytoplasm, and mitochondria.[3] However, it is unclear whether these enzymes regulate NAD levels in these different cell areas because the subcellular components, transporters, and metabolites of NAD have not been fully explored.[4]

Our research is focused on the roles of NMNATs in retinal development. Patients with Leber's congenital amaurosis (LCA), an early-onset retinal photoreceptor degeneration

disease, have several mutations at various positions in *NMNAT1*.[5,6] The mutations of *NMNAT1* in patients with LCA are autosomal recessive, and compound heterozygotes are often identified. *Nmnat1* knockout mice are embryonic lethal, and no biallelic null variants have been identified in patients with LCA,[7] suggesting that NMNAT1 is essential for embryonic development; the mutations in patients with LCA may have residual NMNAT1 activity. Previously, we examined the roles of NMNAT1 during retinal development using short hairpin RNA (shRNA)-mediated depletion of NMNAT1 in mouse retinal explant cultures.[8] NMNAT1-knockdown led to large numbers of apoptotic retinal progenitor cells and increased the levels of acetylated histones H3 and H4 in pro-apoptotic genes.[8] These results indicate that NMNAT1 has essential regulatory roles in the expression of apoptosis-related genes that involve histone modification in retinal progenitor cells.

We are interested in identifying the roles of NMNAT1 for retinal commitment.[9] For that purpose, human induced pluripotent cells (hiPSCs) were used as a model system in this study. Retinal organoid (RO) culture is a three-dimensional cell culture that mimics retinal development. Since the first report of ROs using embryonic stem cells (ESCs),[10] several protocols of RO formation from hESCs and hiPSCs have been reported, with improved efficiency and greater cell diversity.[11–14] In this work, we used hiPSC-derived ROs to examine the roles of NMNAT1 during early retinal development, and generated NMNAT1-knockout (KO) hiPSCs using Clustered Regularly Interspaced Short Palindromic Repeats (CRISPR)/Cas9 technology.

Materials and Methods

Establishment of *NMNAT1* Deficient hiPSCs Using CRISPR/Cas9 System

WTC11 is a human male iPS cell line[15] and was maintained according to the protocol provided in the following site: https://labs.gladstone.org/conklin/protocols.html. To establish *NMNAT1* knockout WTC11, the target site of guide RNA (gRNA) was designed by using CRISPRdirect (https://crispr.dbcls.jp/). The ATG initiation codon of *NMNAT1* was localized in exon (Ex) 2; the gRNAs were in introns 1 and 2 (Fig. 1A). The target sequences of gRNAs are as follows: gNMNAT1_#3-1, 5′-cctataactgggctgggcgtggt-3′ and gNMNAT1_#3-2, 5′-cccagtcatgccggttctctagt-3′. Oligo DNAs were hybridized and inserted into the *Bbs*I site of pSpCas9(BB)-2A-GFP (PX458, Addgene, 48138). The gRNAs were expressed by an all-in-one plasmid, which encoded Cas9 and eGFP, along with two gRNAs (Fig. 1B). Construction of PX458 expressing Cas9 VQR variant (D1135V/R1335Q/T1337R) was described previously.[16] WTC11 cells were transfected with the plasmids by Neon Transfection System (Thermo Fisher Scientific). After 2 days of the culture, GFP-expressing cells were sorted by using FACSAria II (BD Biosciences). For the establishment of clonal cell lines, 5×10^3 cells were plated on a 6 well plate, and several colonies derived from a single cell were picked up and clonally expanded. Genomic polymerase chain reaction (PCR) was carried out using PrimeSTAR GXL DNA polymerase (Takara, R050). Knockout of the targeted region was examined by genomic polymerase chain reaction (Supplementary Figs. S1A, S1B), followed by sequencing to confirm that Ex2 (containing the first ATG) was deleted (Fig. 1C). The primer sequences used for genomic PCR and Sanger sequencing are as follows: 5′-aacgcttgaggatacgctcc-3′ and 5′-gtggaaggatacacatgaaactgt-3′.

EdU Labeling of iPSCs and Flow Cytometry, and Measurement of NAD Content

The iPSCs were cultured in Essential 8 (E8) media (Gibco) supplemented with 5-ethynyl-2′-deoxyuridine (EdU) at 10 µM as final concentration for 2 hours before fixation. After the iPSCs were permeabilized, detection of EdU was performed according to the instructions of the Click-iT EdU Flow Cytometry Assay Kits (Thermo Fisher Scientific, Click-iT EdU Alexa Fluor 488 Flow Cytometry Assay Kit, C10425). About 20 colonies were used for each sample, and essentially the same design of the experiments were repeated 3 times. Then, the incorporated EdU into the cells was analyzed using FACS Aria SORP (BD Biosciences) and CellQuest software (BD Biosciences).

NAD content in retinal organoids was measured using AmpliteTM Fluorimetric NAD/NADH Ratio Assay Kit (AAT Bioquest), according to the manufacturer's instructions. Briefly, retinal organoids at indicated developmental stages were harvested and dissociated with accutase (Nakalai). Then, measurement of NAD contents was performed in accord with the manufacturer's instructions. The values of NAD content were normalized by the cell number.

Induction of Retinal Organoids From WTC11-NMNAT1-KO hiPSC and NAD Supplementation

The hiPSC derived retinal organoid culture was performed based on the previously published protocol.[17] Briefly, WTC11 or WTC11-NMNAT1-KO hiPSCs were harvested and resuspended in E8 media supplemented with 10 µM Y27632 (Fujifilm Wako Pure Chemical Co.) and seeded in V-bottom 96-well plate (1200 cells in 1 well)[17] to form the embryoid body (EB). Until day 7 of the culture, the E8 media was replaced with neural-induction media (NIM1) gradually, as described previously.[17] Then, the aggregates were transferred onto the Matrigel (Corning, 356231)-coated dishes, and were cultured until day 16. Then, the NIM1 was replaced with neural-induction media 2 (NIM2) to expand the retinal primordium. At day 21, the aggregates were detached and served to floating culture. We administrated NMN (Tokyo Chemical Industry) or NAD (Tokyo Chemical Industry) into culture media at 1 µM or 100 nM as the final concentration for the phenotypic rescue experiments. Until starting the differentiation culture, hiPSCs were maintained in the normal culture media, then, NMN or NAD was added at 1 µM or 100 nM as the final concentration at the initial day of the differentiation culture. NMN or NAD was present during all the culture periods at the same final concentration until the cells were harvested. NMN or NAD was replaced with new reagent when culture medium was refreshed; every day in the initial 3 weeks, and once for 2 days in the following culture.

RNA Extraction, cDNA Synthesis, and Quantitative Polymerase Chain Reaction

Immature hiPSCs in one well of the 24-well plate and about 10 colonies of differentiating hiPSCs were used for one condition. Four independent samples were prepared

Investigative Ophthalmology & Visual Science

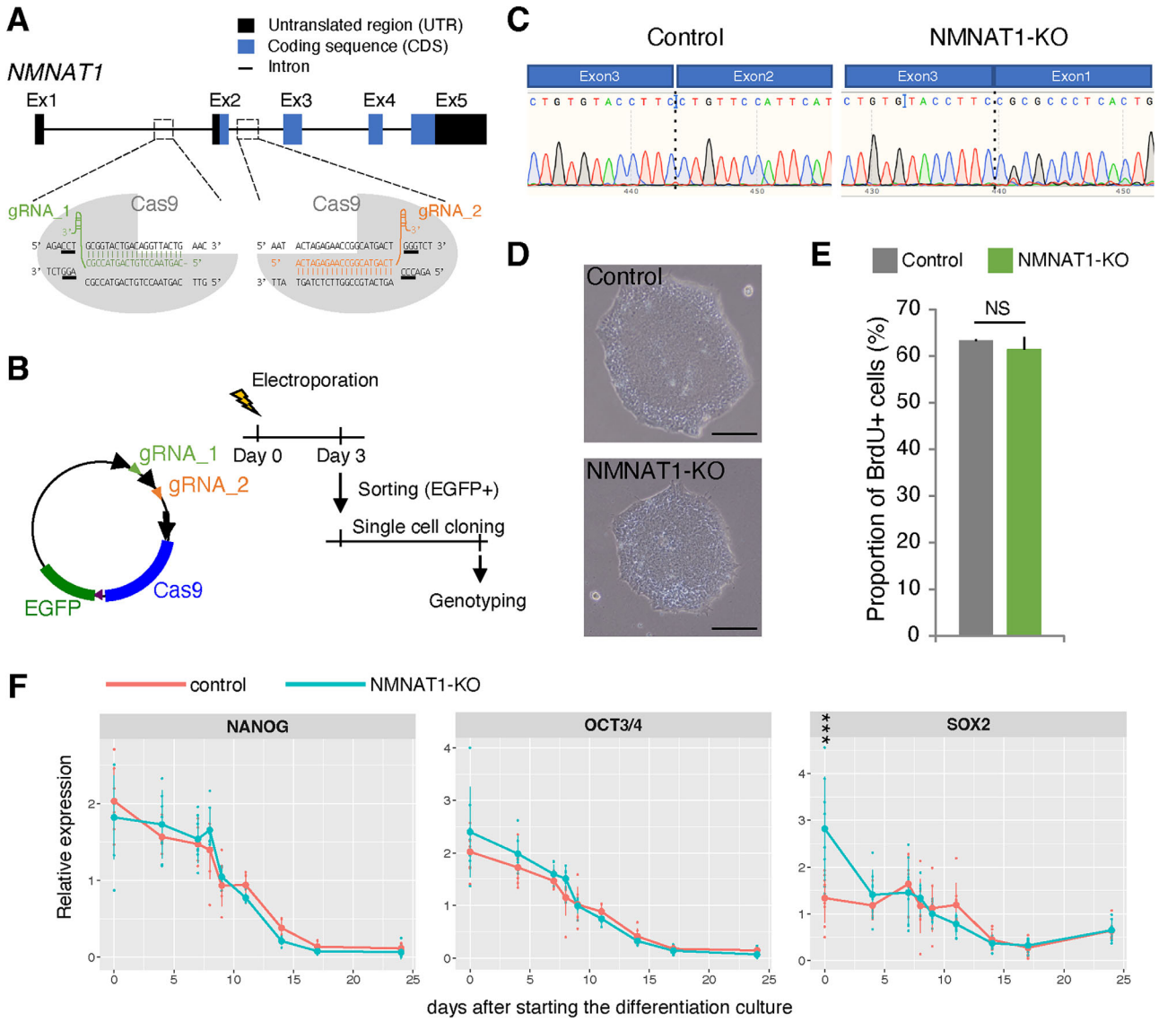

Figure 1. Generation of NMNAT1 knockout hiPSCs. (**A**) Design of gRNAs to knockout NMNAT1 in hiPSCs. (**B**) Schematic representation of the plasmid and experimental schedule to establish NMNAT1-KO hiPSC clones. (**C**) DNA sequence profile to confirm deletion of the exon2 of NMNAT1 in hiPSC clones. (**D**) Bright field photographs of immature hiPSC clones of control and NMNAT1-KO. Scale bars are 100 µM. (**E**) Cell proliferation of hiPSCs was examined by EdU incorporation. (**F**) Transition of gene expression during retinal organoids culture of control or NMNAT1-KO clones. Retinal organoids were harvested at 0, 4, 7, 8, 9, 11, 14, 17, and 24 days after starting the culture, and RT-qPCR was performed on cDNA prepared from the harvested organoids. Values are average of three (**E**) or eight (**F**) independent samples with the standard deviation. Statistical analysis was done by students' *t*-test (**E**) or 1-way ANOVA followed by Tukey's honestly significant difference (HSD) multiple-comparison test (**F**). *** $P < 0.01$ (**F**).

for each condition. Total RNA was purified from samples by using Sepasol RNA I Super G (Nacalai Tesque, Japan), and cDNA was synthesized using ReverTra Ace qPCR RT Master Mix (Toyobo, Japan). Quantitative polymerase chain reaction (qPCR) was performed by the SYBR Green-based method with the Roche Light Cycler 96 (Roche Diagnostics, Japan). For the normalization, the relative expression levels were calculated by using the expression level of *GAPDH*. Then, the average of the relative values of all time points of the control samples (quadruplicates × 9 time points) of each gene was calculated. Final data were obtained by dividing each relative value of control or NMNAT1-KO samples by the average value of the corresponding control samples of each gene. Therefore, the average of the control samples in qPCR is 1 in all the graphs. The primer sequences are listed below unless the sequences were previously reported.[8] *NMNAT1*, 5′-gcacctcaggttgtttgagc-3′, 5′-ggcatcaccaacaggagaga-3′, *NMNAT2*, 5′-ctcagtcacacaccccaac-3′, 5′-gagacaggaagaacggcgtc-3′, *NANOG*, 5′-ctcccatcctacggatgcac-3′, 5′-tacgtgatgacagcatcggg-3′, *OCT3/4*, 5′-caatggtgtgacgcaggga-3′, 5′-ggactggatgttctgggtctg-3′, *SOX1*, 5′-agcgaaccagtatcgagaacc-3′, 5′-ctgatctgctgcagtgtggg-3′, *SOX2*, 5′-aatactggagacgaacgccg-3′, 5′-aacccaagtctggtgtcagc-3′, *PAX6*, 5′-tgctgcacatttgggcg-3′, 5′-tgcagaaatgtgctgctgtg-3′, *OTX2*, 5′-attgctagagcagccctcac-3′, 5′-ggttcagagtccttggtggg-3′, *VSX2*, 5′-agtgtcatggcggagtatgg-3′, 5′-ttttgtgcatccccagtagc-3′, *NEUROD1*, 5′-ctgctcaggacctactaacaacaa-3′, 5′-gtccagcttggaggacctt-3′, *RAX*, 5′-ccctaagcgtgctttcagga-3′, 5′-tttgctcaggaccgacagac-3′,

POU4F2, 5′-cctttcctcgtccgctcttt-3′, 5′-gttcgctccctcttcagtcc-3′, *TUBB3*, 5′-attctggtggacctggaacc-3′, 5′-gacccttggcccagttgtt-3′, *ELAVL3*, 5′-tctgaccccaatgatgcagac-3′, 5′-acgtacaggttagcatcc cg-3′, *SIX3*, 5′-ggtttaagaaccggcggcag-3′, 5′-tcggtccaatggcct ggt-3′, *CRX*, 5′-ccttctgacagctcggtgtt-3′, 5′-tggtgtacttcagcgg tcac-3′, *NR2E3*, 5′-agacaatctcgccaaaggca-3′, 5′-tgtgctcaca gagaagccag-3′, *HES1*, 5′-agaaggcggacattctggaaa-3′, 5′-cctcgttcatgcactcgct-3′, *GAPDH*, 5′-tgaccacagtccatgccatc-3′, and 5′-cataccaggaaatgagcttgac-3′.

Immunohistochemistry

Immunohistochemistry of frozen sections was done as described previously.[18,19] Primary antibodies used were mouse monoclonal antibodies against Ki67 (BD Biosciences, #55060924), TUBB3 (R&D Systems, MAB1195), goat polyclonal antibody against human BRN3B (Santa Cruz, sc-60267), CRX (Abnova Corp., 4G11, H00001406-M02), RXRG (Santa Cruz, A-2, sc-365252), and chick polyclonal antibody against GFP (Abcam, ab13970). Secondary antibodies used were Alexa Fluor 488 or Alexa Fluor 594 conjugated appropriate secondary antibodies (Life Technologies, USA). At least a few colonies for one condition were stained, and representative data are shown in the figures. For section immunohistochemistry, a few sections from three independent colonies were stained, and representative data are shown in the figures. Photographs were taken under observation using Zeiss Axio Image M1 and Axio Image M2 (Carl Zeiss, Germany).

Single Cell RNA Sequencing and Quality Control

We dissociated retinal organoids differentiated from control hiPSCs and NMNAT1-KO hiPSCs at 7 days and 24 days of culture using accutase and collected 5000 to 10,000 cells from each sample using a cell sorter, FACS Aria II (BD Biosciences). Then, the libraries were prepared by using Chromium Next GEN Single Cell 3′ Kit version 3.1 (10× Genomics). Briefly, single-cell suspensions were loaded onto a Chromium Controller (10× Genomics) to generate Gel Bead-in-Emulsion (GEMs). Reverse transcription, cDNA amplification, and library construction were performed according to the manufacturer's protocol. The libraries were served for the sequence on an Illumina NovaSeq6000. After the sequencing, quality control and adapter trimming of the sequenced reads were performed by FastQC (version 0.11.9) and cut adapt (version 3.5). Then, the sequenced reads were pseudoaligned to Homo sapiens transcriptome and the count-matrix was generated using kallisto-bus tools (version 0.46.0).

Data Analysis of Single Cell RNA-Seq

Data analysis of the single-cell RNA sequencing results were performed by using the Scanpy package (version 1.8.2). Our analysis pipeline consists of preprocessing, quality control, normalization, dimensionality reduction, clustering, and differential gene expression analysis. We utilized the Python programming language to implement these steps and generated a comprehensive dataset that captured the transcriptional landscape of individual cells in our sample. To preprocess the data, we performed filtering and normalization steps to remove low-quality cells and genes. We then performed dimensionality reduction using Uniform Manifold Approximation and Projection (UMAP). Using the resulting clusters, we identified cell-type-specific marker genes and annotated each cell based on its expression profile.

Western Blot

Western blot was performed as described previously[8] using total proteins purified from immature hiPSCs corresponding with 1 well of the 24-well plate and about 10 colonies of differentiating hiPSC_ROs were extracted from control or NMNAT1-KO hiPSC derived samples and served for Western blot. Primary antibodies used were mouse monoclonal antibodies against poly ADP ribose (Merck), acetylated lysine (Merck), acetylated HISTONE h3 (Merck, Germany), acetylated HISTONE h4 (Merck, Germany), ACTIN (Merck), goat antibody against NEUROD1 (Santa Cruz), and sheep antibody against VSX2 (Exaplha). Horseradish peroxidase (HRP)-linked_antibody against mouse IgG (GE Healthcare), donkey antibody against sheep IgGP (R&D), and rabbit antibody against goat IgG (Santa Cruz) were used as secondary antibodies. The chemiluminescent signals were detected with Amersham Imager 600 (Fuji Film and Cytiva). Signals were quantified by using ImageJ/Fiji software, and the data were normalized by ACTIN band intensity.

In-Gel Digestion

Total proteins (5 µg) from each sample were separated by an SDS-PAGE, and the gels were stained by using SYPRO Ruby Gel Stains (Sigma Aldrich). Portions of the gels above the 220 kDa marker indicated by molecular weight markers (MagicMark XP Western Protein Standard, ThermoFisher) were cut into 5 parts. These gel fragments were independently digested, and sliced into 1 mm^2 cubes, and washed with H_2O for 5 times. To remove staining, 50% CH_3CN in 100 mM NH_4HCO_3 solution was added to the samples after incubation for 10 minutes at 37°C. Then, 100% CH_3CN was added to remove H_2O, and the samples were incubated for another 10 minutes at 37°C. After drying gels by Speed Vac (Thermo Fisher Scientific), the samples were reduced in 10 mM DTT for 15 minutes at 50°C and alkylated in 10 mM iodoacetamide for 15 minutes at room temperature in the dark. Then, the samples were digested overnight with trypsin (Promega) at 37°C. Peptides were extracted with 50% CH_3CN, 0.1% TFA/20% HCOOH, 25% CH_3CN, and then, 15% IPA/80% CH_3CN solutions, and dried by Speed Vac and dissolved in 0.2% TFA/2% CH_3CN solution.

Mass Spectrometry

Peptides were analyzed using the Orbitrap Fusion ETD mass spectrometer (Thermo Fisher) coupled to a nanoLC (Michrom Bioresources, Auburn, CA, USA) with a column L-column 2 micro C18 column 3 µm, 200 Å, 150 × 0.2 mm i.d. (CERI, Tokyo, Japan). Chromatographic effluents were: A, 99.9% CH3CN/0.1% HCOOH:: and B, 100% CH_3CN. The column was developed at a flow rate of 1.0 µL/min, with a concentration gradient of CH_3CN: from 5% B to 30% B for 100 minutes, and then from 30% B to 95% B for 2 minutes, maintained at 95% B for 8 minutes, from 95% B to 5% B for 2 minutes, and finally re-equilibrated with 5% B for 8 minutes. Effluents were introduced into the mass spectrometer via a nanoelectrospray ion interface that held the separation column outlet directly connected to a Dream Spray electrospray ion source. The electrospray ionization voltage

Investigative Ophthalmology & Visual Science

was 1.8 kilovolt (kV), and the transfer capillary of the orbitrap inlet was heated to 280°C. No sheath or auxiliary gas was used. The mass spectrometer was operated in a data-dependent acquisition mode, in which the mass spectrometer acquisition with a mass range of m/z 390 to 1590 was automatically switched to tandem mass spectrometer acquisition under the automated control of the Xcalibur software. The top 20 precursor ions were selected by a mass spectrometer scan with Orbitrap at a resolution of 240,000, and for the subsequent tandem mass spectrometer scans through an ion trap in the normal/centroid mode, using the AGC mode with AGC values of 2 × 105 and 1 × 104 for full mass spectrometer and tandem mass spectrometer, respectively. We also used a dynamic exclusion capability that allowed sequential acquisition of the tandem mass spectrometer of abundant ions in the order of their intensities with an exclusion duration of 5 seconds and exclusion mass widths of −5 and +5 ppm. The trapping time was 35 ms with the auto gain control on.

Statistical Analysis

The *P* values were calculated by two-tailed Student's *t*-test or 1-way ANOVA followed by Tukey's multiple-comparison test, as indicated in the legends to the Figures 1, 3, 5.

Data Availability

Nucleotide sequence data reported are available in the DDBJ/EMBL/GenBank databases under the accession number(s) DRA011441.

Results

Loss of NMNAT1 Was Not Essential for hiPSC Survival and Proliferation

We generated NMNAT1-KO clones of human iPSCs using the CRISPR-Cas9 system, as described in the Materials and Methods section. The gross morphology of immature NMNAT1-KO hiPSCs clones was indistinguishable from the gross morphology of the control clones (Fig. 1D). We used two independent clones (#393 and #398) for subsequent analyses and obtained similar results. The following figures in this paper show representative data obtained using #398. Proliferation activity, examined by the EdU assay, was comparable between the control and NMNAT1-KO hiPSCs (Fig. 1E). The expression levels of transcripts of the pluripotential genes, *NANOG* and *OCT3/4*, were also similar between the control and NMNAT1-KO hiPSCs (Fig. 1F, day 0), suggesting that NMNAT1 knockout does not affect the nature of immature hiPSCs. However, the level of *SOX2* was higher in NMNAT1-KO hiPSCs than in control hiPSCs (see Fig. 1F).

Induction of Retinal Lineage via Formation of Organoids From NMNAT1-KO hiPSCs

We examined the effects of NMNAT1 knockout in hiPSCs during retinal lineage differentiation, and adapted a previously published protocol for RO formation from hiPSCs.[17] We harvested the organoids at various time points after starting the culture, and reverse transcription quantitative real-time polymerase chain reaction (RT-qPCR) was performed. The levels of *NANOG* and *OCT3/4* decreased in a similar manner during differentiation in the ROs derived from the control and NMNAT1-KO hiPSCs (see Fig. 1F). The initial level of *SOX2* was much higher in NMNAT1-KO hiPSCs than in the control hiPSCs; however, *SOX2* expression rapidly decreased after differentiation began, and it became indistinguishable from the control at day 4 (see Fig. 1F).

Bright-field microscopy showed that the gross morphologies of the embryoid bodies in the control and NMNAT1-KO hiPSCs were similar on day 7 and day 11 (Fig. 2A). On day 14, colonies in the control hiPSCs began to exhibit the formation of neuroblast-like structures (see Fig. 2A, red arrowheads, Supplementary Fig. S2C); however, the morphologies of colonies in the NMNAT1-KO hiPSCs were similar to the morphologies on day 11 (see Fig. 2A, Supplementary Fig. S2C). On day 21, several transparent neuroblast-like structures appeared in the control hiPSCs colonies, but not in NMNAT1-KO hiPSCs colonies. Additionally, the control hiPSCs colonies expanded outward; the colony area was much narrower for NMNAT1-KO hiPSC colonies than for control hiPSC colonies (see Supplementary Figs. S2A, S2B). The colonies were picked and moved to a suspension culture. After 8 weeks, retinal-like organoids were observed in the control hiPSCs derived samples, but no translucent neuroblastic structures were observed in the NMNAT1-KO hiPSCs derived samples (see Fig. 2A).

Next, we examined the expression of the neural protein marker TUBB3 by immunostaining. On day 15, strongly TUBB3-positive fine-shaped neuron-like cells were localized and scattered along the outside edges of NMNAT1-KO hiPSC-derived colonies (Fig. 2B). In contrast, strongly TUBB3-positive fine-shaped neuron-like cells were clustered immediately outside of control colonies (see Fig. 2B). On day 21, the clustered TUBB3-positive cells formed neuroblast-like structures in the control colonies; in contrast, TUBB3-positive neuron-like cells were scattered toward the outside edges of NMNAT1-KO colonies (Fig. 2C).

We examined the proliferation and differentiation of retinal ganglion cells (RGCs), one of the earliest differentiation subtypes in the retina, by immunostaining (Fig. 2D). Ki67, proliferation antigen, signals were localized toward the outer third of the area of control ROs, corresponding to the neuroblastic layer of the early developing retina (see Fig. 2D). RGC marker BRN3B signals were observed inside control ROs, corresponding to the region where RGCs typically localize (see Fig. 2D). In contrast, NMNAT1-KO ROs showed a small number of Ki67-positive cells scattered across the whole colony area (see Fig. 2D). BRN3B signals were also scattered across the whole RO area (see Fig. 2D), suggesting the failure of the layered structure formation in NMNAT1-KO_ROs. Quantification of the signals of Figure 2D was done by ImageJ software. KI67 and BRN3B values, which were normalized by DAPI signals, of control_KI67, NMNAT1-KO_KI67, control_BRN3B, and NMNAT1-KO BRN3B, are 0.383, 0.065, 0.185, and 0.163, respectively. We also examined the expression of CRX, which marks the rod and cone, and RXRG, which is a marker protein of cone, respectively, by immunohistochemistry of the frozen sections. We found the expression of both CRX and RXRG in the control sections, but not in the NMNAT1-KO sections (Fig. 2E). We hypothesized that embryoid body formation occurred in a similar manner in the control and NMNAT1-KO hiPSCs; however, differentiation to the retinal lineage was severely disrupted by the absence of NMNAT1.

Investigative Ophthalmology & Visual Science

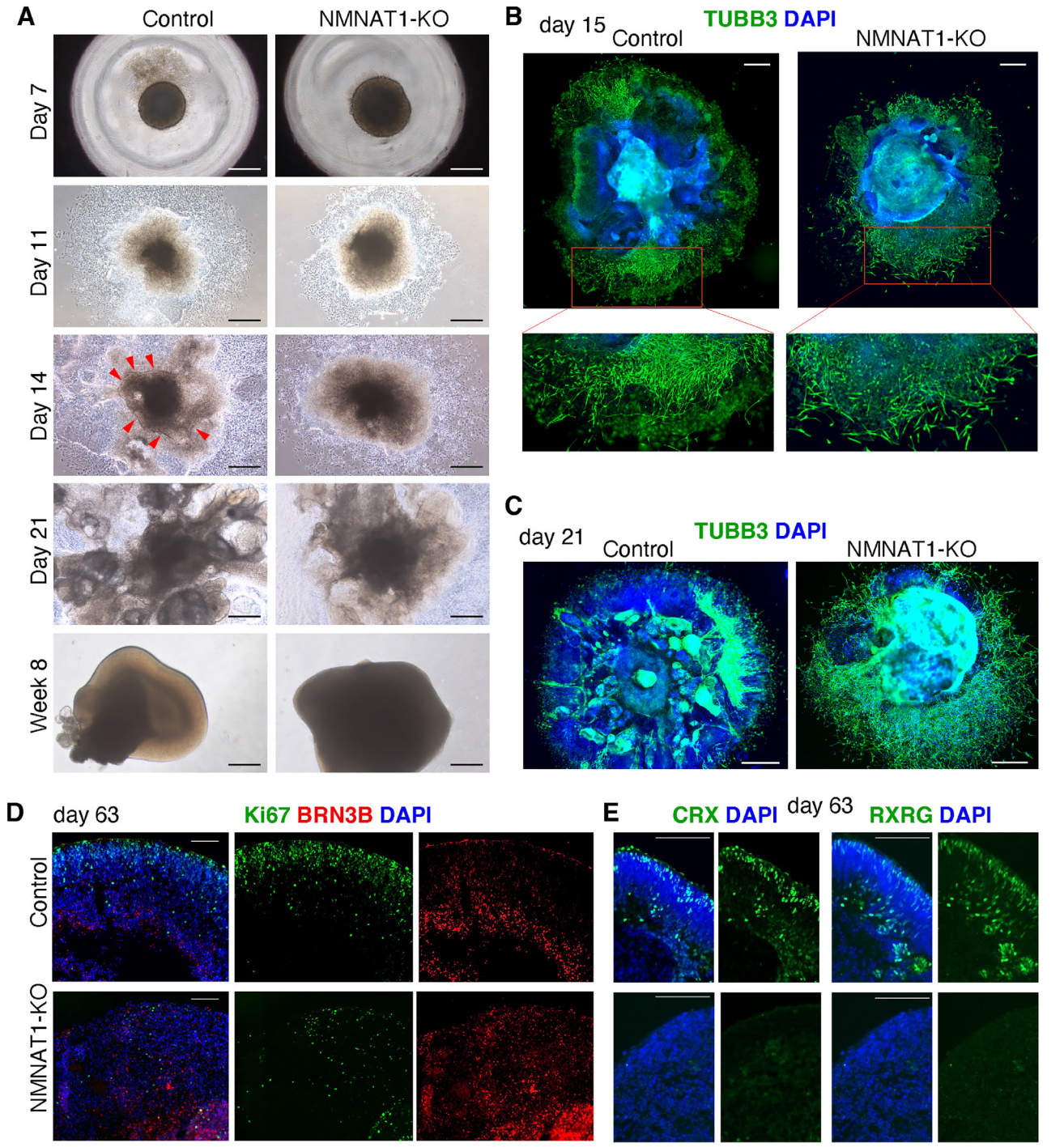

Figure 2. Induction of retinal organoids from NMNAT1-KO hiPSC. (**A**) Bright field photographs of the retinal organoids made from control or NMNAT1-KO hiPSCs were taken at the cultured days 7, 11, 14, and 21, and week 8. Representative photographs from 10 to 20 colonies of few independent cultures are shown. (**B, C**) Colonies at day 15 (**B**) and 21 (**C**) were immunostained with anti-TUBB3 antibody, and nuclei were visualized by DAPI staining. In **B**, the *red square regions* of *upper panels* are enlarged in the *lower panels*. Representative photographs of six samples from two independent cultures are shown. (**D, E**) Colonies at day 63 were frozen sectioned, and the sections were immunostained with anti-Ki67 and -BRN3B antibodies (**D**), or anti-CRX or -RXRG antibodies (**E**). Representative photographs of three sections from three independent organoids of two independent cultures are shown. Nuclei were visualized by staining with DAPI (**B–E**). Scale bars are 500 µm (**A, B, C**) and 100 µm (**D, E**).

Investigative Ophthalmology & Visual Science

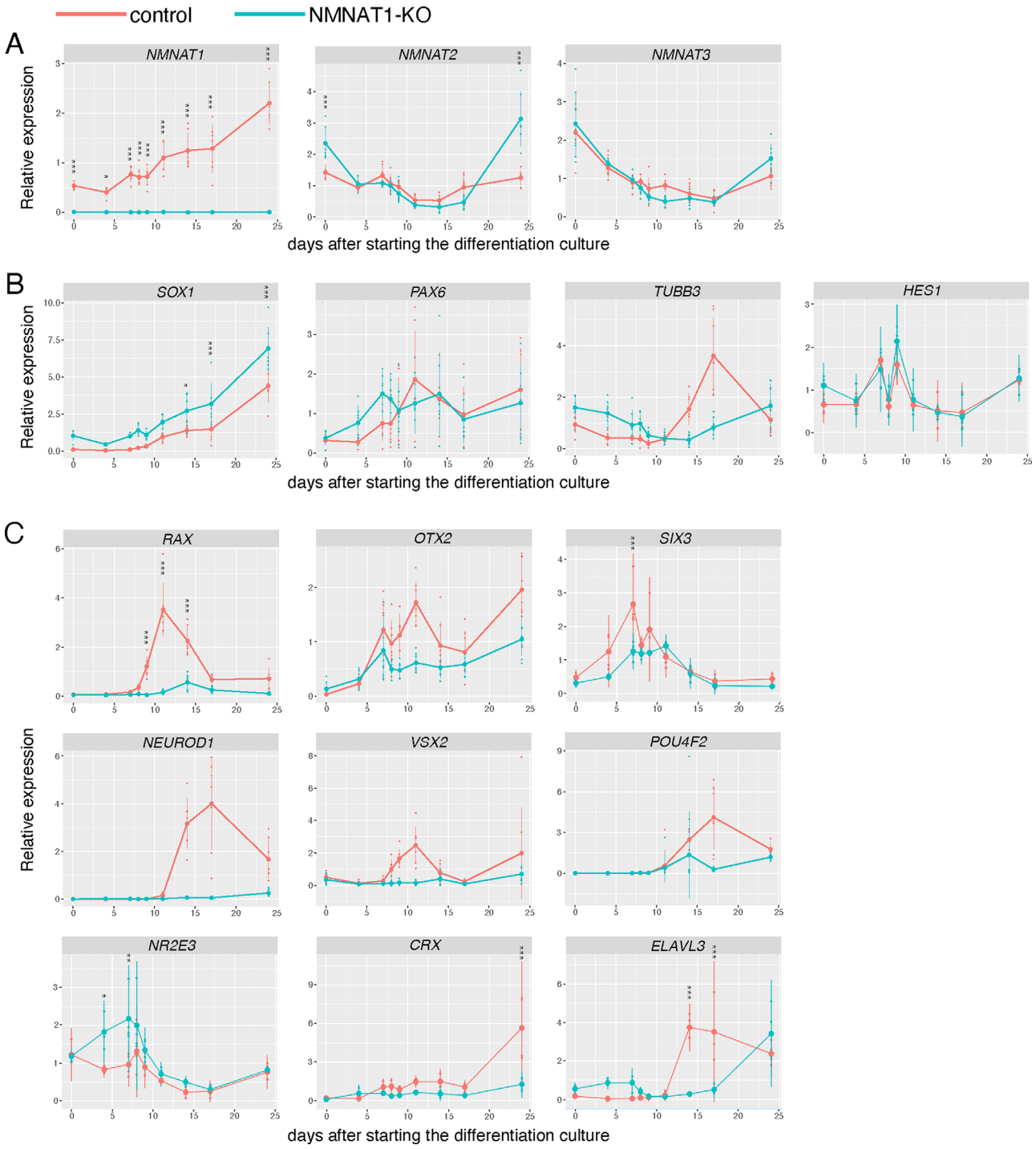

Figure 3. Gene expression patterns during retinal organoid formation. (**A–C**) Retinal organoids were formed from NMNAT1-KO or control hiPSCs, and harvested at 0, 4, 7, 9, 11, 14, 17, and 24 days after starting the organoid culture and served for RT-qPCR. Primers used are to detect *NMNATs* (**A**), neural lineage genes (**B**), and retinal lineage related genes (**C**). Values are average of four independent samples with the standard deviation. The *P* values were calculated by 1-way ANOVA followed by Tukey's honestly significant difference (HSD) multiple-comparison test, * $P < 0.05$, ** $P < 0.005$, *** $P < 0.0005$.

Examination of Gene Expression Patterns During RO Formation

We examined gene expression patterns during RO formation by RT-qPCR. First, we examined the expression patterns of NMNAT family genes. Expression levels of *NMNAT1* transcripts were very low in immature control hiPSCs; these levels increased during RO differentiation (see Fig. 3A). There was no *NMNAT1* expression in the NMNAT1-KO hiPSCs, as expected. *NMNAT2* expression levels were similar until day 17; however, on day 24, *NMNAT2* expression was higher in NMNAT1-KO hiPSCs_ROs than in control

Investigative Ophthalmology & Visual Science

hiPSCs_ROs (see Fig. 3A). *NMNAT3* expression in control and NMNAT1-KO hiPSCs gradually decreased until day 17 (see Fig. 3A).

Next, we examined neural development-related genes. SOX1 is an early responder to neural-inducing signals and a marker of neural induction.[20,21] *SOX1* levels began to increase on day 7 in control and NMNAT1-KO hiPSCs; they were higher in NMNAT1-KO hiPSC_ROs than in control ROs after 14 days of culture (see Fig. 3B). PAX6 is uniformly expressed in early neural ectoderm[22] as well as in retinal progenitors and essential for retinal development.[23] *PAX6* expression gradually increased, beginning immediately after culture initiation, in the control and NMNAT1-KO hiPSCs (see Fig. 3B). TUBB3 is a marker of neural lineage[24] and is expressed in various early retinal cell subtypes, such as cone, horizontal, and amacrine cells.[25] *TUBB3* expression was slightly higher in NMNAT1-KO hiPSCs colonies until a few days after culture initiation; however, it sharply increased in the colonies of control hiPSCs but not in NMNAT1-KO hiPSCs (see Fig. 3B). *HES1* is involved in neurogenesis by various ways,[26] and we found that *HES1* expression levels were similar between control and NMNAT1-KO samples (see Fig. 3B).

RAX plays key roles in the proliferation and differentiation of early retinal progenitor cells[27,28]; in control hiPSCs colonies, its expression sharply increased after 7 days of culture. In contrast, in NMNAT1-KO hiPSCs colonies, there was only a slight increase in expression on day 14 (see Fig. 3C). *RAX* expression in control hiPSCs colonies sharply decreased after 11 days, consistent with previous observations that *RAX* is only transiently expressed in mouse early retinal progenitor cells.[29] *OTX2* and *SIX3*, which are also required for eye field formation,[30,31] increased in the control, and NMNAT1-KO_ROs showed lower levels of expression (see Fig. 3C). Notably, *RAX* and *OTX2* expression levels peaked at the same time (day 11), suggesting that day 11 is a critical period for retinal lineage commitment, and NMNAT1 is essential for this process.

VSX2 (CHX10) and NEUROD are expressed in retinal progenitor cells.[32,33] In the control hiPSC_ROs, *VSX2* was transiently upregulated around day 11, then downregulated; it increased again after 17 days (see Fig. 3C). These transitional changes in expression were not observed in NMNAT1-KO ROs (see Fig. 3C). After 11 days of culture, *NEUROD1* expression levels sharply increased in control hiPSCs but not NMNAT1-KO hiPSC samples (see Fig. 3C). Protein levels of VSX2 and NEUROD1 were examined by Western blotting, and we found that lower expression levels of these proteins in NMNAT1-KO samples at day 11 or 17 (Supplementary Fig. S3). POU4F2, which is expressed in RGCs, increased approximately 17 days in control hiPSCs ROs. However, this expression peak was not observed in NMNAT1-KO_ROs (see Fig. 3C). NR2E3 and CRX are critical transcription factors in photoreceptor fate determinant.[34,35] *NR2E3* showed higher expression levels in NMNAT1-KO samples at few days after starting the differentiation culture, and *CRX* levels were upregulated at day 24 in control but not in NMNAT1-KO samples. ELAVL3 is a pan-amacrine marker and involved in its differentiation,[36] and upregulation of *ELAVL3* observed in the control sample was not observed in the NMNAT1-KO sample (see Fig. 3C). These data indicate that escape from the immature state and neurogenesis of hiPSCs both occur in NMNAT1-KO hiPSCs, whereas retinal specification was at least partly impaired and does not proceed appropriately.

Single-Cell RNA-Sequence Analysis of NMNAT1-KO hiPSCs Derived ROs

We conducted single-cell RNA sequence (scRNA-seq) analysis of control and NMNAT1-KO_ROs on days 7 and 24. The UMAP clustering with Scanpy software (Python) revealed seven clusters (Supplementary Fig. S4A). Examination of the expression patterns of various immature or neural cell marker genes in the 7 clusters showed that characteristic expression patterns in the cluster 0, and 2 to 6, but not in the cluster 1 (see Supplementary Fig. S4B, red arrow head). The hierarchical cluster dendrogram showed close relation of the clusters 5, 2, and 4, and the clusters 6, 0, and 3, but the cluster 1 was located distant from these 2 groups (see Supplementary Fig. S4B). We designated the cluster 1 as unknown, and removed the cluster 1 from the following analyses. Using the remaining six clusters, we analyzed the expression patterns of additional several marker genes (see Supplementary Figs. S4C, S4D). Cluster 5 strongly expresses several neural markers, and we designated this cluster as neurons (Neu). The clusters 0, 3, and 6 have characteristic expression of immature markers, *POU5F1*, *SOX2*, and *NANOG*, and we designated these clusters as pluripotent cell populations 1, 2, and 3 (PPCs_1, 2, and 3), respectively (see Supplementary Figs. S4B–D). The clusters 2 and 4 do not show strong expression of the immature markers, but expressed moderate levels of neural markers: therefore, we designated the clusters as neural progenitor cells 1 and 2 (NPCs_1 and 2), respectively. The top 10 strongly expressed genes in the clusters are shown in Figure 4A.

The breakdown of 4 sample populations; days 7 and 24 of control_ and NMNAT1-KO_RO showed that the sum of PPCs_1 (cluster 0), PPCs_2 (cluster 3), and PPCs_3 (cluster 6) constituted about 90% of control_ and NMNAT1-KO_ROs on day 7; but these populations disappeared from both samples on day 24, as expected (Fig. 4B). NPCs_1 (cluster 2) is about 10% in both control and NMNAT1-KO samples at day 7, and NPCs_1 consists of about 60 and 80% in day 24 control_ and NMNAT1-KO_ROs, respectively. Population of NPCs_2 and Neu are much higher in control than in NMNAT1-KO samples (see Fig. 4B), suggesting that the retinal lineage cells are included in these populations. It is notable that a small population of Neu cluster exist in the NMNAT1-KO samples but not in the control at day 7 (see Fig. 4B, red arrowhead), suggesting this population may reflect premature differentiation of NMNAT1-KO cells to the neural lineage. The breakdown of the cluster categories showed smaller population of NPCs_2 and Neu in NMNAT1-KO samples at day 24, supporting the idea that the retinal lineage cells are included in these populations (see Fig. 4C).

To address the developmental relationships among the clusters, we assessed pseudotemporal trajectories by processing UMAP by using Force Atlas2[37] (Fig. 4D). Distribution of the clusters showed the developmental changes from the cluster 3 (PPCs_2) and 0 (PPCs_1) to condensed cluster 5 (Neu) population through the cluster 2 (NPCs_1) and the cluster 4 (NPCs_2) (Fig. 4E). When the 4 samples (days 7 and 24 of control and NMNAT1-KO samples) are assigned in the pseudotime graph layout, it appeared that day 24_control-ROs are assigned in the main population of Neu, and a part of day 24_NMNAT1-KO samples are assigned in a tip small population which is different population from that of control day 24 samples. Small populations of NMNAT1-KO on day 7 were also present in this area, supporting premature differentiation of neurons in NMNAT1-KO cells (Fig. 4F).

Investigative Ophthalmology & Visual Science

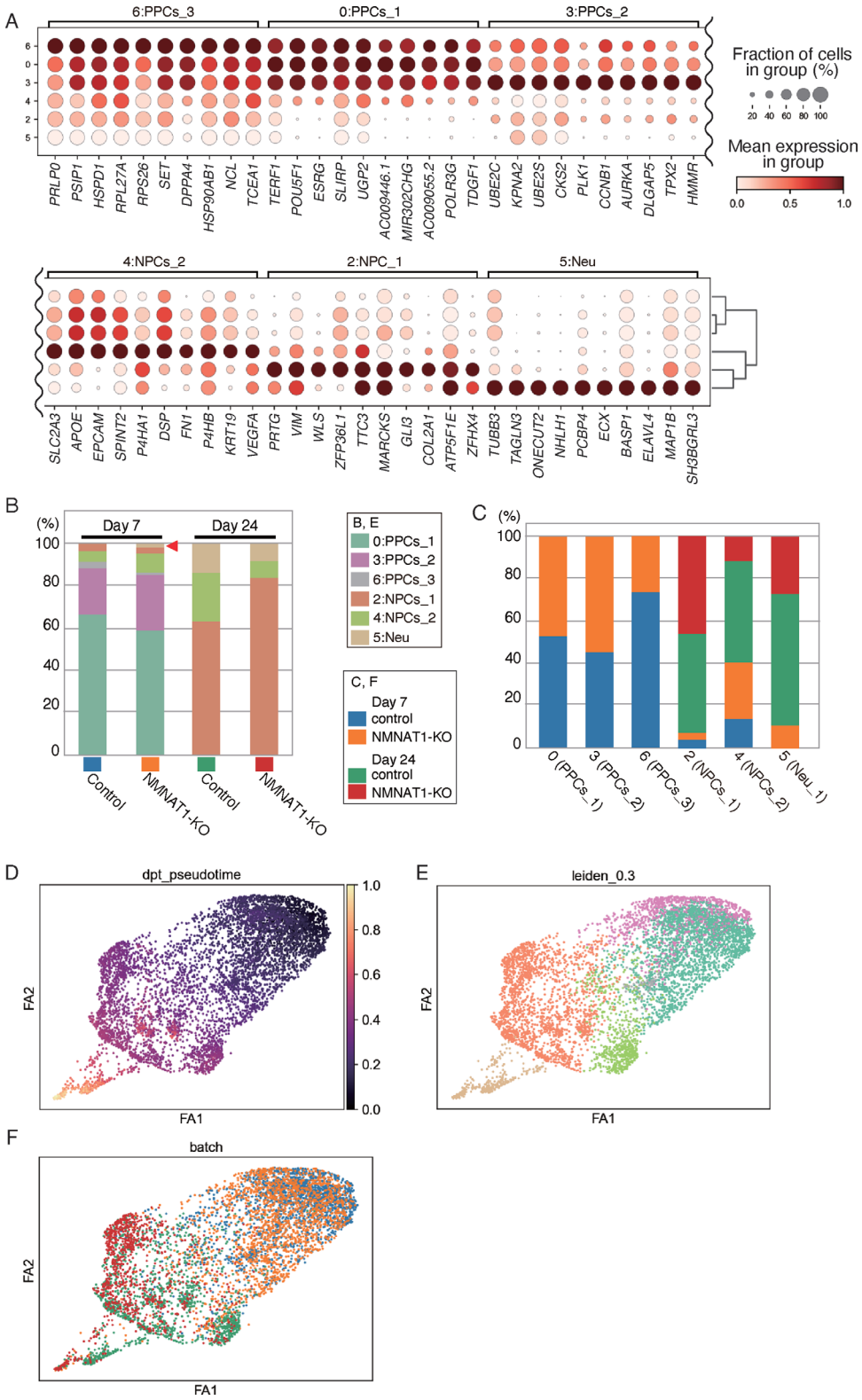

Figure 4. Single cell transcriptome of NMNAT1-KO and control retinal organoids. The single cells collected from control and NMNAT1-KO retinal organoids at day 7 and day 24 were served for single cell RNA-seq. (**A**) Dot blot representing the top 10 strongly expressed genes in each cluster. Relative values of gene expressions in the six clusters are represented by the color and size of the dot. The color of each dot represents the expression level of each gene (mean expression in the group). The size of each dot corresponds to the percentage of cells in the cluster expressing the gene (fraction of cells in the group). (**B**) The composition of the 6 clusters in the population of control_ and NMNAT1-KO_ROs at day 7 or day 24. (**C**) The proportion of samples (control_ and NMNAT1-KO_ROs at day 7 and day 24) that contributes to each cluster. (**D–F**). Pseudotime estimation of differentiation processes from immature to retinal/neural lineage was performed by mapping of UMAP cell clusters by Force Atlas2. The dpt_pseudotime annotation representing transition from immature to neural differentiation processes (**D**). Cells of 7 clusters are visualized in the FA1/FA2 space (**E**). Mapping of the cells of the control_ and NMNAT1-KO_RO at day 7 and day 24 in the FA1/FA2 space (**F**).

Investigative Ophthalmology & Visual Science

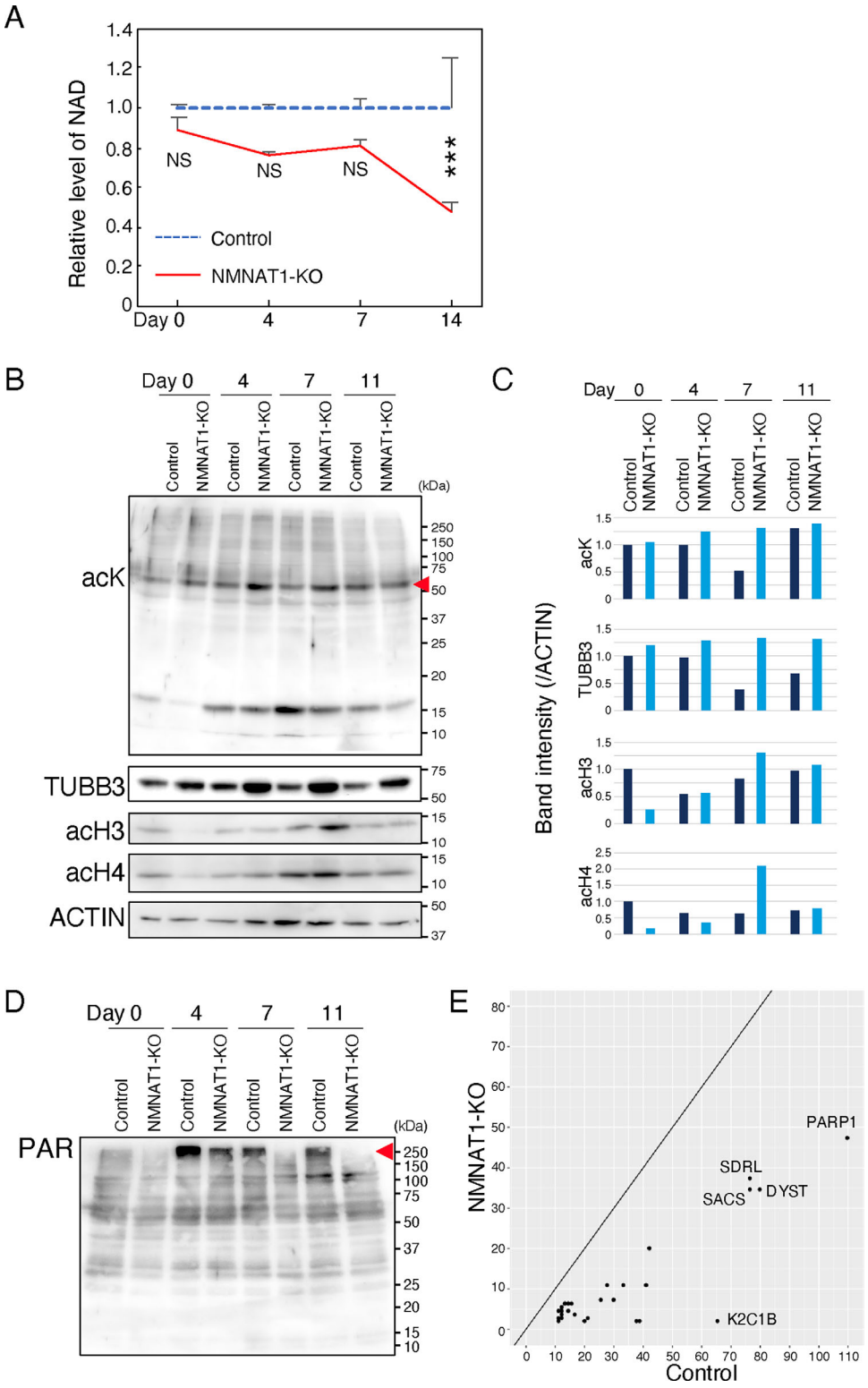

Figure 5. Changes in NAD level and post-translational modification in NMNAT1-KO hiPSCs. (**A**) Chronological changes of NAD level during RO formation were examined in the control and NMNAT1-KO by colorimetric methos. The iPSCs (day 0) and the ROs at the indicated time points (days 4, 7, and 14) were harvested, and NAD contents were measured using AmpliteTM Fluorimetric NAD/NADH Ratio Assay Kit. The values are the average of three or four independent samples with standard deviation. Statistical significance was calculated by 1-way ANOVA followed by Tukey's honestly significant difference (HSD) multiple-comparison test. NS, not significant, *** $P < 0.005$. (**B-D**) Total proteins were extracted from the ROs at the indicated time points. Western blotting using acetylated lysine (**B**), -TUBB3 (**B**), -acetylated histone H3 (acH3, **B**), -acetylated histone H4 (acH4, **B**), ACTIN (**B**) and anti-poly ADP ribose (**D**) antibodies at time points days 0, 4, 7, and 11. Signals of acK, TUBB3, acH3, and acH4 were quantified by using ImageJ software (**C**). (**E**) The abundance of proteins with a molecular weight of 220 kDa or greater that showed changes in PARylation levels between control and NMNAT1KO was analyzed by liquid chromatography–tandem mass spectrometry. Scatterplot shows peptide counts for proteins that showed peptide counts of 10 or higher in control and whose abundance was reduced to less than half in NMNAT1-KO.

Investigative Ophthalmology & Visual Science

Table. Identification of PARylated Proteins With Molecular Weight Equivalent About 200 kDa or Greater

Identified Proteins	Accession Number	Molecular Weight	Control	NMNAT1-KO	Fold Change	Total Peptide Count
Sortilin-related receptor	SORL_HUMAN	248 kDa	76.46	37.36	2.05	113.82
Phosphate carrier protein, mitochondrial	MPCP_HUMAN	40 kDa	13.30	6.38	2.08	19.67
Terminal uridylyl transferase 4	TUT4_HUMAN	185 kDa	13.30	6.38	2.08	19.67
Small subunit processome component 20 homolog	UTP20_HUMAN	318 kDa	42.11	20.05	2.10	62.15
Sacsin	SACS_HUMAN	521 kDa	76.46	34.62	2.21	111.08
Protocadherin fat 1	FAT1_HUMAN	506 kDa	12.19	5.47	2.23	17.66
Receptor-type tyrosine-protein phosphatase eta	PTPRJ_HUMAN	146 kDa	12.19	5.47	2.23	17.66
Protocadherin fat 3	FAT3_HUMAN	502 kDa	14.41	6.38	2.26	20.78
NAD(P) transhydrogenase, mitochondrial	NNTM_HUMAN	114 kDa	14.41	6.38	2.26	20.78
Dystonin	DYST_HUMAN	861 kDa	79.78	34.62	2.30	114.41
Poly [ADP-ribose] polymerase 1	PARP1_HUMAN	113 kDa	109.70	47.38	2.32	157.08
Zinc finger protein 462	ZN462_HUMAN	285 kDa	15.51	6.38	2.43	21.89
Alanine–tRNA ligase, cytoplasmic	SYAC_HUMAN	107 kDa	11.08	4.56	2.43	15.64
TATA-binding protein-associated factor 172	BTAF1_HUMAN	207 kDa	27.70	10.93	2.53	38.64
Sickle tail protein homolog	SKT_HUMAN	214 kDa	12.19	4.56	2.68	16.74
MAX gene-associated protein	MGAP_HUMAN	336 kDa	12.19	4.56	2.68	16.74
Cluster of STE20-like serine/threonine-protein kinase	SLK_HUMAN [2]	143 kDa	12.19	4.56	2.68	16.74
STE20-like serine/threonine-protein kinase	SLK_HUMAN	143 kDa	12.19	4.56	2.68	16.74
FACT complex subunit SPT16	SP16H_HUMAN	120 kDa	33.24	10.93	3.04	44.18
Anaphase-promoting complex subunit 1	APC1_HUMAN	217 kDa	14.41	4.56	3.16	18.96
Kinesin-like protein KIF20B	KI20B_HUMAN	211 kDa	12.19	3.64	3.34	15.83
Tyrosine-protein phosphatase non-receptor type 13	PTN13_HUMAN	277 kDa	25.49	7.29	3.50	32.77
Cluster of Kinesin-like protein KIF21A	KI21A_HUMAN [2]	187 kDa	41.00	10.93	3.75	51.93
Kinesin-like protein KIF21A	KI21A_HUMAN	187 kDa	41.00	10.93	3.75	51.93
Probable helicase senataxin	SETX_HUMAN	303 kDa	11.08	2.73	4.05	13.81
DNA (cytosine-5)-methyltransferase 1	DNMT1_HUMAN	183 kDa	29.92	7.29	4.10	37.21
Serine/threonine-protein kinase MRCK beta	MRCKB_HUMAN	194 kDa	12.19	2.73	4.46	14.92
Cluster of Keratin, type II cuticular Hb6	KRT86_HUMAN [2]	53 kDa	11.08	2.00	5.54	13.08
Dedicator of cytokinesis protein 1	DOCK1_HUMAN	215 kDa	21.05	2.73	7.70	23.79
Chromodomain-helicase-DNA-binding protein 9	CHD9_HUMAN	326 kDa	19.95	2.00	9.97	21.95
Putative heat shock protein HSP 90-beta 4	H90B4_HUMAN	58 kDa	37.68	2.00	18.84	39.68
RANBP2-like and GRIP domain-containing protein 8	RGPD8_HUMAN	199 kDa	38.78	2.00	19.39	40.78
Keratin, type II cytoskeletal 1b	K2C1B_HUMAN	62 kDa	65.38	2.00	32.69	67.38
Proliferation marker protein Ki-67	KI67_HUMAN	359 kDa	16,621.00	3.64	4560.57	16,624.64

Identification of Downstream Factors in NAD-NMNAT1-PARP Cascade by Liquid Chromatography–Tandem Mass Spectrometry

We examined the NAD levels during RO formation, and the difference levels between control and NMNAT1-KO samples gradually increased, and the level was significantly lower in NMNAT1-KO than levels in the control group on day 14 (see Fig. 5A). These findings do not contradict the consistent increase in NMNAT1 levels in the control group (see Fig. 3A). We used a biochemical approach to clarify the downstream mechanism in NMNAT1-KO samples. We examined acetyl-lysine and acetyl histones H3 and H4 by Western blotting (see Fig. 5B) because these are NAD-dependent biochemical reactions. There was a slight increase in the band corresponding to 50 kDa in the acetyl-lysine blot and a similar tendency in the anti-TUBB3 blot, which has a position equivalent to the acK approximately 50 kDa band (see Fig. 5B, red arrowhead). We also observed several bands of varying intensity between the control and NMNAT1-KO samples in the acetyl-lysine, acH3, and acH4 blots. However, the differences were relatively small and inconsistent with days 4, 7, and 11 samples (see Fig. 5B). Quantification results of the Western blotting are shown in Figure 5C.

ADP-ribosylation is critical for post-translational modification in various cell processes and requires NAD.[38,39] The band equivalent to the 250 kDa protein displayed changes in PARylation levels (see Fig. 5D, red arrowhead). We extracted proteins with molecular weights of approximately 200 kDa or greater and performed liquid-chromatography tandem mass spectrometry for identification (Supplementary Fig. S6). We compared the identified proteins between the control and NMNAT1-KO samples, revealing 34 proteins with >10 peptide counts in control samples; these counts were reduced to less than half in NMNAT1-KO samples (see the Table, Fig. 5E). PARP1 was most abundant in the control and NMNAT1-KO samples (see the Table, Fig. 5E). PARP1, a poly(ADP)-ribosyl transferase, catalyzes auto-PARylation modification on its own amino acid residues.[40,41] Therefore, we speculate that PARP1 is a target affected by NMNAT1 knockout in hiPSCs.

Roles of NAD in the Retinal Differentiation of hiPSCs

Exogenous NAD rescued the mouse retinal phenotype induced by expression of shRNA targeting *Nmnat1*.[8] Because NAD levels were lower in NMNAT1-KO_ROs (see Fig. 5A), we examined whether the addition of NAD or

Investigative Ophthalmology & Visual Science

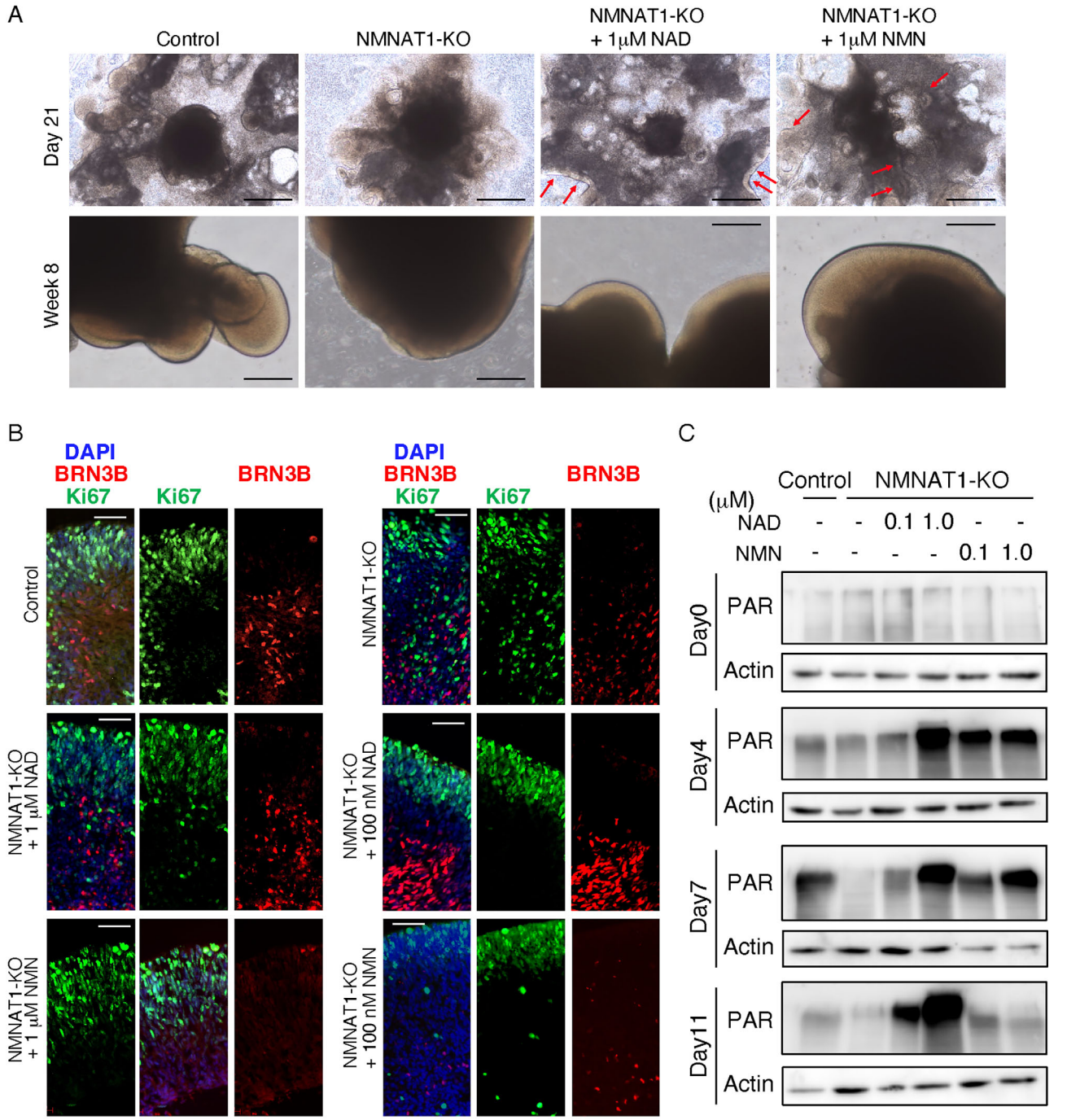

Figure 6. NMNAT1-KO retinal organoids phenotype was restored by supplementation of NAD or NMN. (**A–C**) Retinal organoid culture of control or NMNAT1-KO hiPSCs was performed in the presence of NAD or NMN. (**A**) Bright field images of the NMNAT1-KO ROs cultured in the presence or absence of NAD (1 μM) or NMN (1 μM) and control ROs at 21 days (*upper panels*) and 8 weeks (*lower panels*) are shown. Scale bars = 500 μM. (**B**) The retinal organoids of control or NMNAT1-KO hiPSCs in the presence of absence of NAD (1 μM or 100 nM) or NMN (1 μM or 100 nM) at 8 weeks were harvested and frozen sectioned. The sections were stained with anti-Ki67, and -BRN3 antibodies, and nuclei were visualized by DAPI staining. Scale bars = 50 μM. (**C**) Retinal organoids were formed from control or NMNAT1-KO hiPSCs with the indicated culture condition. Total proteins were extracted from retinal organoids at indicated days, and poly(ADP-ribosyl)ation (PARylation) level was examined by Western blotting. PARylation levels equivalent to 250 kDa, which were lost in NMNAT1KO, showed a concentration-dependent recovery with the addition of NAD or NMN.

NMN reversed the NMNAT1-KO-induced phenotype. NAD or NMN (at final concentration of 1 μM) was added to the RO culture medium; retinal neuroblast-like structures formed in NAD- or NMN-supplemented NMNAT1-KO_ROs on day 21 (Fig. 6A, red arrows). At week 8, there were retina-like structures in floating cultures of NAD- or NMN-supplemented NMNAT1-KO_ROs (see Fig. 6A). Immunohistochemical analysis of control ROs at 8 weeks revealed the

Investigative Ophthalmology & Visual Science

presence of Ki67 and BRN3B in the outer and inner RO halves, respectively (Fig. 6B). NMNAT1-KO_ROs displayed no such layered structure; however, the addition of NAD or NMN resulted in Ki67 signals in the outer half of each RO, as observed in the control RO (see Fig. 6B). Although the NAD-supplemented sample showed BRN3B signals in the inner half, no such signals were present in NMN-supplemented samples. A similar tendency was observed when the samples were supplemented with 100 nM of NAD or NMN (see Fig. 6B). Western blotting showed that decreased levels of poly(ADP-ribosyl)ation (PARylation) equivalent to 250 kDa were recovered by supplementation with NAD or NMN (Fig. 6C). Intriguingly, 1 µM of NAD or NMN showed stronger bands than 100 nM NAD or NMN (see Fig. 6C).

Discussion

This study identified the essential role of NMNAT1 in committing hiPSCs to the retinal lineage, but NMNAT1 is not required to maintain the characteristics of immature hiPSCs. *NMNAT1* expression levels in immature hiPSCs were very low. However, they increased during RO formation after a few days of culture, consistent with the observation that abnormalities in NMNAT1-KO hiPSC_ROs were evident a few days after RO culture initiation.

The expression level of *NMNAT1* significantly increased after 7 days of culture; subsequently, retinal early progenitor-expressing genes such as *RAX* and *OTX2* dramatically increased their expression levels around day 10. Pax6, Six3, Otx2, Sox2, Vsx2, and Rax are essential for retinal development.[42,43] Mutations in *RAX* or *OTX2* were detected in the genomes of patients with anophthalmia or microphthalmia.[44–46] There was almost complete suppression of *RAX* and *VSX2* and severe suppression of *OTX2* in NMNAT1-KO hiPSC_ROs. The expression of early differentiated retinal subtype-specific genes, such as *NEUROD1* and *POU4F2* in NMNAT1-KO hiPSC_ROs, was also considerably reduced. Germline deletion of Rax in mice resulted in anophthalmia (absence of eyes).[27] Conversely, ectopic expression of Rax in mouse ES cells led to the ability to differentiate into retinal subpopulations when ES cells were grafted into mouse retina.[18] Therefore, the lack of RAX in NMNAT1-KO_ROs may have caused the failure of retinal-specific gene induction and retinal differentiation. Studies using *Xenopus laevis* have indicated roles for Otx2 and Sox2 in Rax transcriptional induction,[47,48] but transcriptional regulation of *RAX* genes in mammals is not yet fully understood. The scRNA-seq analysis showed that small cell populations in the UMAP space (see the lower projection in Fig. 4B) may be very early retinal lineage cells. However, no cells were mapped in sample populations from day 7. This result suggests that retinal primordial cells appear during a limited transitional span, presumably on days 8 to 9.

Notably, transitions of *NMNAT2* and *NMNAT3* expression levels during RO culture were completely different from the transition of *NMNAT1* in control hiPSCs. On day 25, there was significantly greater expression of *NMNAT2* in NMNAT1-KO hiPSC_ROs than in control hiPSC_ROs. Compensatory expression of NMNAT2 in the absence of NMNAT1 cannot be excluded; however, previous reports did not support functional redundancy of NMNAT1, 2, and 3.[49–51] In addition, our results imply NMNAT1-specific functions are involved in retinal fate determination.

We identified PARP1 as a candidate molecule among downstream NAD-dependent nuclear enzymes necessary for the retinal specification of iPSC-derived ROs. PARP1 catalyzes the poly(ADP)-ribosylation of proteins involved in various physiological processes.[40] Elevated PARP1 levels were observed in the retinas of patients with diabetes; inhibition of PARP1 activity blocks the development of diabetic complications, including neuropathy and retinopathy,[52] highlighting the importance of appropriate PARP1 levels. PARP1 is also involved in light-induced photoreceptor injury, where it repairs damaged DNA, but overactivation of PARP1 can trigger PARP-dependent photoreceptor death.[53] The expression levels of *Parp1* transcripts were high in mouse retinas on embryonic day 14, and the level steadily decreased during retinal development,[8] suggesting that PARP1 has a role in early retinal development. We identified severe loss of PARP1 PARylation in NMNAT1-KO ROs; the levels recovered after the addition of exogenous NAD or NMN. PARP1 functions alone or in a complex with NMNAT1 or HPF1.[39,54] The recovery of proliferation and differentiation upon addition of exogenous NAD suggests a link between PARP1 and these biological events. The recent studies revealed the detailed and complex molecular mechanisms of PARP1 and its related molecules through ADP-ribosylation.[39] The involvement of PARP1 in transcriptional regulation of retinal genes, especially *RAX*, via chromatin remodeling is critical question for examining the roles of the NMNAT1-NAD-PARP1 axis in retinal fate determination.

Acknowledgments

The authors are grateful to Bruce Conklin for providing hiPS cells and fruitful discussion.

Supported by JSPS KAKENHI grant Number 18K16919 (H.K.), 22K09762 (H.K.), 20K18376 (H.K.), 21K09693 (S.W.), and 16H06279 (PAGS).

Disclosure: **H. Kuribayashi**, None; **T. Iwagawa**, None; **A. Murakami**, None; **T. Kawamura**, None; **Y. Suzuki**, None; **S. Watanabe**, None

References

1. Covarrubias AJ, Perrone R, Grozio A, Verdin E. NAD+ metabolism and its roles in cellular processes during ageing. *Nat Rev Mol Cell Biol*. 2021;22(2):119–141.
2. Imai S, Guarente L. It takes two to tango: NAD+ and sirtuins in aging/longevity control. *NPJ Aging Mech Dis*. 2016;2:16017.
3. Berger F, Lau C, Dahlmann M, Ziegler M. Subcellular compartmentation and differential catalytic properties of the three human nicotinamide mononucleotide adenylyltransferase isoforms. *J Biol Chem*. 2005;280:36334–36341.
4. Cambronne XA, Stewart ML, Kim DH, et al. Biosensor reveals multiple sources for mitochondrial NAD+. *Science*. 2016;352:1474–1477.
5. den Hollander AI, Roepman R, Koenekoop RK, Cremers FPM. Leber congenital amaurosis: genes, proteins and disease mechanisms. *Prog Retin Eye Res*. 2008;27(4):391–419.
6. Yi Z, Li S, Wang S, Xiao X, Sun W, Zhang Q. Clinical features and genetic spectrum of NMNAT1-associated retinal degeneration. *Eye (Lond)*. 2022;36(12):2279–2285.
7. Bedoni N, Quinodoz M, Pinelli M, et al. An Alu-mediated duplication in NMNAT1, involved in NAD biosynthesis, causes a novel syndrome, SHILCA, affecting multiple tissues and organs. *Hum Mol Genet*. 2020;29(13):2250–2260.

Investigative Ophthalmology & Visual Science

8. Kuribayashi H, Baba Y, Iwagawa T, Arai E, Murakami A, Watanabe S. Roles of Nmnat1 in the survival of retinal progenitors through the regulation of pro-apoptotic gene expression via histone acetylation. *Cell Death Dis*. 2018;9:891.
9. Adler R, Canto-Soler MV. Molecular mechanisms of optic vesicle development: complexities, ambiguities and controversies. *Dev Biol*. 2007;305(1):1–13.
10. Eiraku M, Takata N, Ishibashi H, et al. Self-organizing optic-cup morphogenesis in three-dimensional culture. *Nature*. 2011;472(7341):51–58.
11. Capowski EE, Samimi K, Mayerl SJ, et al. Reproducibility and staging of 3D human retinal organoids across multiple pluripotent stem cell lines. *Development*. 2019;146(1):dev171686.
12. Chichagova V, Dorgau B, Felemban M, Georgiou M, Armstrong L, Lako M. Differentiation of retinal organoids from human pluripotent stem cells. *Curr Protoc Stem Cell Biol*. 2019;50(1):e95.
13. Fligor CM, Huang K-C, Lavekar SS, VanderWall KB, Meyer JS. Differentiation of retinal organoids from human pluripotent stem cells. *Methods Cell Biol*. 2020;159:279–302.
14. Móvio MI, de Lima-Vasconcellos TH, Dos Santos GB, et al. Retinal organoids from human-induced pluripotent stem cells: from studying retinal dystrophies to early diagnosis of Alzheimer's and Parkinson's disease. *Semin Cell Dev Biol*. 2023;144:77–86.
15. Kreitzer FR, Salomonis N, Sheehan A, et al. A robust method to derive functional neural crest cells from human pluripotent stem cells. *Am J Stem Cell*. 2013;2:119–131.
16. Iwagawa T, Masumoto H, Tabuchi H, Tani K, Conklin BR, Watanabe S. Evaluation of CRISPR/Cas9 exon-skipping vector for choroideremia using human induced pluripotent stem cell-derived RPE. *J Gene Med*. 2023;25(2):e3464.
17. Zhong X, Gutierrez C, Xue T, et al. Generation of three-dimensional retinal tissue with functional photoreceptors from human iPSCs. *Nat Commun*. 2014;5:4047.
18. Tabata Y, Ouchi Y, Kamiya H, Manabe T, Arai K, Watanabe S. Specification of the retinal fate of mouse embryonic stem cells by ectopic expression of Rx/rax, a homeobox gene . *Mol Cell Biol*. 2004;24(10):4513–4521.
19. Iida A, Shinoe T, Baba Y, Mano H, Watanabe S. Dicer plays essential roles for retinal development by regulation of survival and differentiation. *Invest Ophthalmol Vis Sci*. 2011;52(6):3008–3017.
20. Pevny LH, Sockanathan S, Placzek M, Lovell-Badge R. A role for SOX1 in neural determination. *Development*. 1998;125(10):1967–1978.
21. Baharvand H, Mehrjardi N-Z, Hatami M, Kiani S, Rao M, Haghighi M-M. Neural differentiation from human embryonic stem cells in a defined adherent culture condition. *Int J Dev Biol*. 2007;51(5):371–378.
22. Zhang X, Huang CT, Chen J, et al. Pax6 is a human neuroectoderm cell fate determinant. *Cell Stem Cell*. 2010;7(1):90–100.
23. Ashery-Padan R, Gruss P. Pax6 lights-up the way for eye development. *Curr Opin Cell Biol*. 2001;13(6):706–714.
24. Katsetos CD, Herman MM, Mörk SJ. Class III beta-tubulin in human development and cancer. *Cell Motil Cytoskeleton*. 2003;55(2):77–96.
25. Sharma RK, Netland PA. Early born lineage of retinal neurons express class III beta-tubulin isotype. *Brain Res*. 2007;1176:11–17.
26. Dhanesh SB, Subashini C, James J. Hes1: the maestro in neurogenesis. *Cell Mol Life Sci*. 2016;73(21):4019–4042.
27. Mathers PH, Grinberg A, Mahon KA, Jamrich M. The Rx homeobox gene is essential for vertebrate eye development. *Nature*. 1997;387:603–607.
28. Mathers PH, Jamrich M. Regulation of eye formation by the Rx and pax6 homeobox genes. *Cell Mol Life Sci*. 2000;57(2):186–194.
29. Bailey TJ, El-Hodiri H, Zhang L, Shah R, Mathers PH, Jamrich M. Regulation of vertebrate eye development by Rx genes. *Int J Dev Biol*. 2004;48(8-9):761–770.
30. Beby F, Lamonerie T. The homeobox gene Otx2 in development and disease. *Exp Eye Res*. 2013;111:9–16.
31. Diacou R, Nandigrami P, Fiser A, Liu W, Ashery-Padan R, Cvekl A. Cell fate decisions, transcription factors and signaling during early retinal development. *Prog Retin Eye Res*. 2022;91:101093.
32. Donovan SL, Dyer MA. Regulation of proliferation during central neuvous system development. *Semin Cell Dev Biol*. 2005;16:407–421.
33. Ahmad I, Acharya HR, Rogers JA, Shibata A, Smithgall TE, Dooley CM. The role of NeuroD as a differentiation factor in the mammalian retina. *J Mol Neurosci*. 1998;11(2):165–178.
34. Toms M, Ward N, Moosajee M. Nuclear receptor subfamily 2 group E member 3 (NR2E3): role in retinal development and disease. *Genes (Basel)*. 2023;14(7):1325.
35. Tran NM, Chen S. Mechanisms of blindness: animal models provide insight into distinct CRX-associated retinopathies. *Dev Dyn an Off Publ Am Assoc Anat*. 2014;243(10):1153–1166.
36. Wu M, Deng Q, Lei X, Du Y, Shen Y. Elavl2 regulates retinal function via modulating the differentiation of amacrine cells subtype. *Invest Ophthalmol Vis Sci*. 2021;62(7):1.
37. Jacomy M, Venturini T, Heymann S, Bastian M. ForceAtlas2, a continuous graph layout algorithm for handy network visualization designed for the Gephi software. *PLoS One*. 2014;9(6):e98679.
38. Wu X, Xu M, Geng M, et al. Targeting protein modifications in metabolic diseases: molecular mechanisms and targeted therapies. *Signal Transduct Target Ther*. 2023;8(1):220.
39. Dasovich M, Leung AKL. PARPs and ADP-ribosylation: deciphering the complexity with molecular tools. *Mol Cell*. 2023;83(10):1552–1572.
40. Krishnakumar R, Kraus WL. The PARP side of the nucleus: molecular actions, physiological outcomes, and clinical targets. *Mol Cell*. 2010;39:8–24.
41. Zhu T, Zheng J-Y, Huang L-L, Wang Y-H, Yao D-F, Dai H-B. Human PARP1 substrates and regulators of its catalytic activity: an updated overview. *Front Pharmacol*. 2023;14:1137151.
42. Rodgers HM, Huffman VJ, Voronina VA, Lewandoski M, Mathers PH. The role of the Rx homeobox gene in retinal progenitor proliferation and cell fate specification. *Mech Dev*. 2018;151:18–29.
43. Zagozewski JL, Zhang Q, Eisenstat DD. Genetic regulation of vertebrate eye development. *Clin Genet*. 2014;86(5):453–460.
44. Gonzalez-Rodriguez J, Pelcastre EL, Tovilla-Canales JL, et al. Mutational screening of CHX10, GDF6, OTX2, RAX and SOX2 genes in 50 unrelated microphthalmia-anophthalmia-coloboma (MAC) spectrum cases. *Br J Ophthalmol*. 2010;94(8):1100–1104.
45. Chassaing N, Causse A, Vigouroux A, et al. Molecular findings and clinical data in a cohort of 150 patients with anophthalmia/microphthalmia. *Clin Genet*. 2014;86(4):326–334.
46. Voronina VA, Kozhemyakina EA, O'Kernick CM, et al. Mutations in the human RAX homeobox gene in a patient with anophthalmia and sclerocornea. *Hum Mol Genet*. 2004;13(3):315–322.
47. Andreazzoli M, Gestri G, Angeloni D, Menna E, Barsacchi G. Role of Xrx1 in xenopus eye and anterior brain development. *Development*. 1999;126:2451–2460.

Investigative Ophthalmology & Visual Science

48. Zuber ME, Gestri G, Viczian AS, Barsacchi G, Harris WA. Specification of the vertebrate eye by a network of eye field transcription factors. *Development*. 2003;130(21):5155–5167.
49. Zhou T, Kurnasov O, Tomchick DR, et al. Structure of human nicotinamide/nicotinic acid mononucleotide adenylyltransferase. *J Biol Chem*. 2002;277:13148–13154.
50. Raffaelli N, Sorci L, Amici A, Emanuelli M, Mazzola F, Magni G. Identification of a novel human nicotinamide mononucleotide adenylyltransferase. *Biochem Biophys Res Commun*. 2002;2002:835–840.
51. Raffaelli N, Pisani FM, Lorenzi T, et al. Characterization of nicotinamide mononucleotide adenylyltransferase from thermophilic archaea. *J Bacteriol*. 1997;179:7718–7723.
52. Sun J, Chen L, Chen R, Lou Q, Wang H. Poly(ADP-ribose) polymerase-1: an update on its role in diabetic retinopathy. *Discov Med*. 2021;32(165):13–22.
53. Li X, Zhang Z, Fan B, Li Y, Song D, Li G-Y. PARP-1 is a potential marker of retinal photooxidation and a key signal regulator in retinal light injury. *Oxid Med Cell Longev*. 2022;2022:6881322.
54. Gibbs-Seymour I, Fontana P, Rack JGM, Ahel I. HPF1/C4orf27 is a PARP-1-interacting protein that regulates PARP-1 ADP-ribosylation activity. *Mol Cell*. 2016;62(3):432–442.